Tian et al. Nanoscale Research Letters (2019) 14:269
https://doi.org/10.1186/s11671-019-3103-y

Nanoscale Research Letters

NANO EXPRESS

One-Drop Self-Assembly of Ultra-Fine Second-Order Organic Nonlinear Optical Crystal Nanowires

Tian Tian[1], Bin Cai[1,2*], Qingqing Cheng[1], Cheng Fan[1], Yanyan Wang[1], Gongjie Xu[1], Fuxing Gu[1], Feng Liao[1], Okihiro Sugihara[2], Eiji Hase[3] and Takeshi Yasui[3]

Abstract

In this study, we propose a one-drop self-assembly method, which proved capable of successfully preparing 4-N, N-dimethylamino-4′-N′-methyl-stilbazolium tosylate (DAST) single-crystalline nanowires (NWs). The apparent roughness of the DAST NWs was determined to be less than 100 pm by using a high-resolution atomic force microscope, indicating their ultrafine quality. The DAST NWs also exhibited excellent nonlinear optical properties, including two-photon excited fluorescence and second harmonic generation, which could enable the production of low-cost, low-power-consumption wideband wavelength conversion devices. Thus, the described method may provide a new avenue for organic NW fabrication.

Keywords: Nanowires, DAST, Nonlinear, Self-assembly

Introduction

Second-order organic nonlinear optical (NLO) materials have ultra-fast electro-optic response times as well as very large bandwidths and NLO coefficients, and therefore, have been intensively researched for a wide range of applications related to electrical/optical signal transduction, optical switching, phased-array radar, analogue/digital conversion, terahertz signal generation, and digital signal processing [1, 2]. Organic ionic 4-N, N-dimethylamino-4′-N′-methyl-stilbazolium tosylate (DAST) crystals are recognized as benchmark organic NLO crystals due to their electro-optic coefficients $\gamma_{11} = 55 \pm 80$pm/V at 1315 nm , high-NLO susceptibilities $\chi^{(2)}(-2\omega, \omega, \omega) = 580 \pm 30$pm/V at 1535 nm, and low-dielectric constants (5.2, 10^3–10^5 kHz) [3, 4] and consequently are researched intensively [5–9]. However, the applications of DAST crystals are limited due to their deficient quality and the difficulty of fabricating DAST crystal optical waveguides using the traditional "top-down" approach. Meanwhile, self-assembly, a bottom-up technique, is becoming a powerful method for fabricating micro/nanoscale one-dimensional (1D) structures and is promising for the production of miniaturized integrated electronic, optoelectronic, and photonic devices [10–12]. For organic materials, the self-assembly driving forces can originate from interactions such as coordination bonding, aromatic π–π stacking, hydrogen bonding, Van der Waals forces, and electrostatic interactions [13–15]. Although many organic materials have been successfully employed to synthesize second harmonic generation (SHG) active 1D crystalline nanostructures, their second-order susceptibilities are still far lower than those of organic NLO crystals with large dipole moments [16]. In this study, we develop an environmentally friendly one-drop self-assembling method for DAST NWs fabrication. We separate crystal seeds preparation and growth process by substrate-supported rapid evaporation crystallization (SSREC) [17, 18] and saturated vapor cultivation respectively. In this way, we can easily obtain ultra-fine single-crystalline DAST NWs with good NLO properties.

* Correspondence: bullcai@usst.edu.cn
[1]Shanghai Key Lab of Modern Optical System, Ministry of Education, University of Shanghai for Science and Technology, Shanghai 200093, China
[2]Graduate School of Engineering, Utsunomiya University, Utsunomiya 321-8585, Japan
Full list of author information is available at the end of the article

Methods

The DAST powder (Daiichi Pure Chem. Co. Ltd.), methanol (99.9%, Surper Dry, with molecular sieves, water ≦ 30 ppm, J&K Seal), and the surfactant (cetyltrimethylammonium bromide, CTAB, TCI) were used directly without further purification.

Preparation

Firstly, 30 mg of DAST powder and 10 mg of the surfactant were dissolved in 5 mL of methanol. Next, 100 μL of this DAST-CTAB methanol solution was diluted with 10 mL of methanol (DAST concentration of approximately 0.146 mM,) and stirred for 0.5 h to obtain a homogeneous solution (for more details, see Additional file 1: Figure S1).

Characterization

The DAST NW morphology was studied using an optical microscope (Imager.A2m, Zeiss), BTEM (Tecnai G2 SpiritBiotwin), SEM (Nanolab600i, Helios, Quanta 200, Fei), and AFM (MultiMode8, Bruker). The UV-Vis spectra were obtained using a fiber spectrometer (Nova, Idea Optics). The crystal structure of the NW was examined using XRD (D/Max 2550 V, Rigaku). The two-photon excited fluorescence (TPEF) was excited using a 1064 nm cw laser (MIL-III-1064-1W, CNI), the images were obtained using an optical microscope (DS-RI2, Nikon), and the emission spectrum was measured using the fiber spectrometer.

The second harmonic generation (SHG) polarization dependence of the DAST NCs was measured using a homemade SHG microscope. A 1250-nm femtosecond laser (Insight DeepSee, Spectra-Physics) with a wavelength of 1250 nm, the repetition rate of 80 MHz, and a pulse width of 130 fs were employed as the light source (for more details, see Additional file 1: Figure S1).

Results and Discussion

A schematic of the one-drop self-assembly method is shown in Fig. 1a. First, the hydrophilic substrate was placed on a hot plate and heated to 80 °C. Then, 100 μL of the 0.146 mM DAST-CTAB methanol solution was dropped onto the heated hydrophilic substrate and heated continuously for 20 s. As the methanol solvent spread and evaporated, the DAST nano/microcrystals (NC/MCs, orange color) were rapidly deposited on the substrate shown in step 1, Fig. 1a. In step 2, the substrate was placed into a culture dish and sealed with approximately 0.1 mL of methanol solvent for the wet-cultivation process. After ~ 3 h of cultivation at room temperature, the DAST NWs (green color) were obtained in step 3. The morphological evolution of the DAST crystals is shown in Fig. 1b–f. The DAST crystals as-deposited appear as micro-flakelets with a relatively high density, and no wires can be observable as shown in Fig. 1b. And then after 40 min of cultivation in the atmosphere of saturated methanol vapor pressure, at room temperature, the shorter DAST rods begin to appear, shown in Fig. 1c.The slice-shaped crystals are smaller than the crystals in Fig. 1b. Furthermore, after 2.5 h of cultivation, some longer DAST crystal wires show up, see Fig. 1e. The DAST wires have uniform widths generally with several hundred micrometers long; some of them could even be longer than 1 mm. There is a microscope image of the DAST wires with the polarizer rotated by 90° in Fig. 1f. The entire tilted wires appear to have been changed from their maximized anisotropy birefringence (brightest) states to their minimal (extinguished) states. This alteration implies that the single crystalline structures of the fabricated DAST wires are highly uniform. Meanwhile, large DAST crystal particles no longer appear, and instead, small crystal dots are visible. Furthermore, the crystal dot density near the DAST wires is obviously lower than the density further away.

Thus, we expect that the DAST wire formation process was as follows. After the SSREC process, small DAST crystals were deposited on the substrate. When they were put into the methanol atmosphere, the DAST crystals absorbed the methanol and partially dissolved into it, resulting in NC/MCs surrounded by a DAST-saturated methanol solution. The self-assembling driven force could originate from the huge dipole moments of NC/MCs [19–21]. For instance, an MC with 0.35-micron diameter may have a dipole moment magnitude as large as ~ 4.5 x 10^4 D. Meanwhile, the methanol solution acts as a lubricant and can facilitate the motion of the DAST NC/MCs. Due to the electrostatic interaction and the lubrication provided by the methanol solution, the DAST NC/MCs undergo self-assembly, yielding DAST NWs. As an evidence, a biology transmission electron microscope (BTEM) image of an unfinished DAST NW is shown in Fig. 1d, plenty of NCs gathered in the NW can be confirmed. As the DAST NWs grow, they continually absorb the nearby DAST solution via the capillary effect. Consequently, as is evident from Fig. 1d, e, the residual crystal dot density near the wires is lower than that further away.

An X-ray diffraction (XRD) pattern of DAST NWs is presented in Fig. 2a. By referring to the crystal cell parameters of bulk DAST crystals (monoclinic Cc space group, point group m, a = 10.365 Å, b = 11.322 Å, $\alpha = \beta = 90°$, and $\gamma = 92.24°$) [4], the diffractive peaks near 10°, 20°, and 30° corresponding to the [002], [004], and [006] faces of the DAST crystals, respectively. It means that DAST NWs grown on the substrate have the [001] orientation with the a- and b-axes along the film plane. The morphologies of the DAST NWs were further studied using an SEM. An SEM image from the [001]

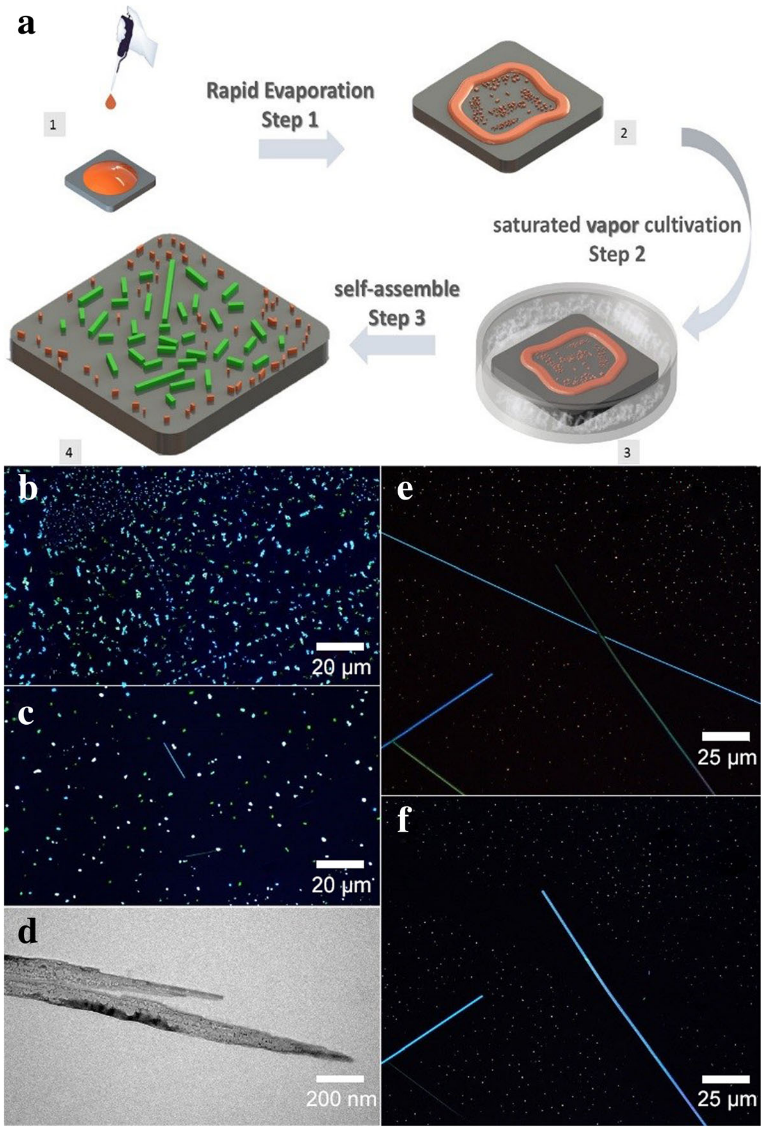

Fig. 1 **a** The schematic of the one-drop self-assembly method. **b** The fluorescence image of DAST crystal after the SSREC process. **c** After 40 min of cultivation in a methanol atmosphere. **d** The BTEM image of unfinished DAST NW. **e** After 2.5 h of cultivation in a methanol atmosphere. **f** After 2.5 h of cultivation in a methanol atmosphere with the cross-polarizer rotated by 90°

perspective is shown in Fig. 2b. Based on the characteristics of bulk DAST crystal growth, the [111], [-111], [1–11], and [110] end faces can be identified easily (see Fig. 2). The single-crystalline DAST NW has a belt-like morphology, with a typical width of 1.5 ± 0.5 μm and thickness of 0.8 ± 0.4 μm. According to the NW's crystal orientation, the alignment of the DAST molecules in the NW can be depicted as in Fig. 2c, the tosylate anions have been removed for clarity. For the DAST, bulky crystal directly grows from saturated DAST solution, the growth speed along the crystallographic *a*-axis is the fastest, in other words, in the [100] direction [22]; however, in the case of self-assembly, the [110] direction has priority. Thus, there is a different mechanism drive the NW fabrication. We expect that the NW formation begins with DAST NC/MC self-assembly due to the electrostatic force. For a four-molecule model, the dipole moments along the *a*-, *b*-, and *c*-axes in a DAST crystal lattice are 158.2 D, 141.2 D, and 121.0 D, respectively [18]. The growth along the *c*-axis was limited due to the configuration of the present experiment, so the NWs could only grow along the direction of the vector sum of the dipole moments of the *a*- and *b*-axes. Since the dipole moments along the *a*- and *b*-axes are similar, the [110] direction become preferred NW growth direction.

To investigate the internal quality of the DAST NWs, we used an electron beam to cut an NW, whose cross-section was shown in Fig. 2d. The white

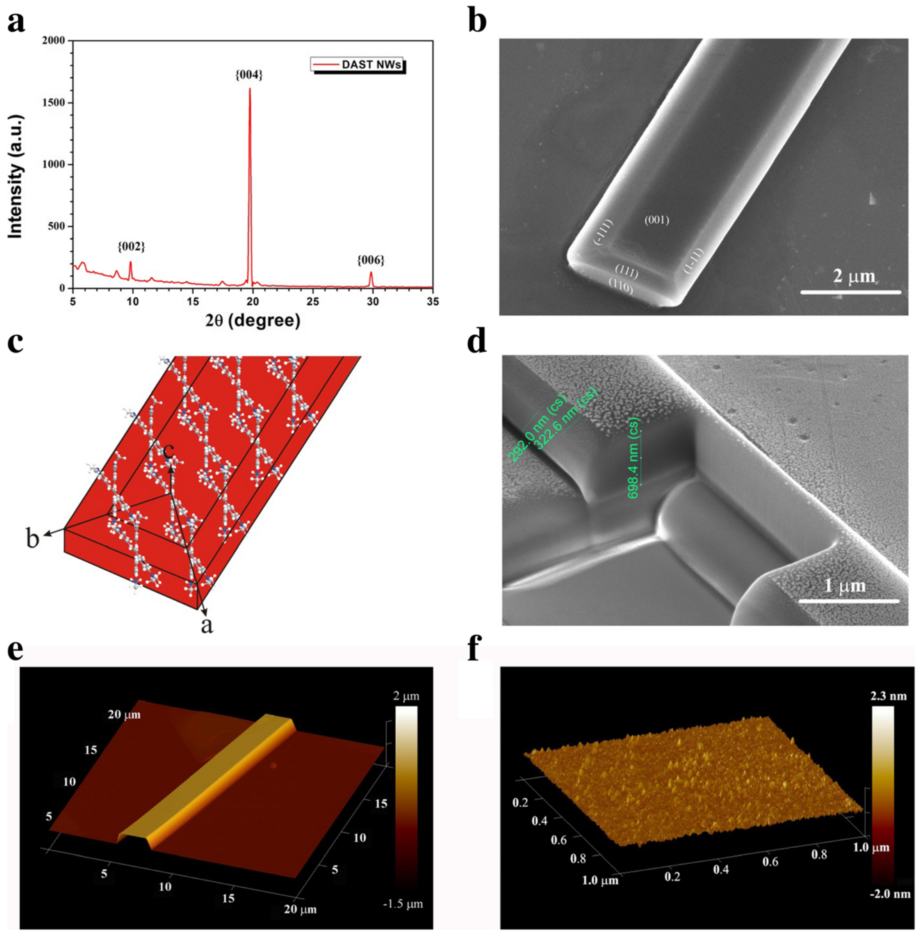

Fig. 2 **a** The XRD pattern of DAST NWs. **b** SEM image of a DAST NW from the [001] perspective, where, based on the typical characteristics of bulk crystal growth, the [-111], [111], [1-11], and [110] faces can be identified. **c** DAST molecular alignment in the NW, where the tosylate anions have been omitted for clarity. **d** The cross-section of a DAST NW cut by a focused ion beam. **e** AFM image of a DAST NW. **e** The surface roughness of a DAST NW, as determined using an AFM

dots on the NW are silver nanoparticles that were deposited to increase the conductivity of the NW. The roughness of the cut cross-section is similar to as-grown DAST crystals, and no defect can be detected at this scale. We further investigated the DAST NW morphology by using a high-resolution atomic force microscope (AFM) to obtain the surface information directly without disturbing the metallic silver nanoparticles. As shown in Fig. 2e, the NW has a clear belt configuration with the [001] face as the flat top surface, which is consistent with the SEM results. By zooming in on the top surface of the DAST NW using the AFM, we obtained the morphology of a 1000 x 1000 nm^2 region of the [001] face, which is presented in Fig. 2f. According to the results, an average roughness of DAST NW is about ~ 85 pm, which is even smaller than that of a graphene monolayer on a SiO_2 substrate [23]; thus, an ultra-flat DAST NW crystal was realized. For a low-loss optical waveguide, its surface roughness must be less than 10 nm. Obviously, our DAST NWs were of much higher quality than required.

The UV-Vis absorption spectrum of the DAST NWs is compared with those of the bulk crystal, NC, and solution states in Fig. 3a. Due to the unique 1D conformation of the NW, its absorption spectrum (black line) is obviously different from those of the other states. In methanol solution, an absorption peak at ~ 476 nm [8, 17] is originated from the π-conjugation system of DAST cation. Upon crystallization, due to the electronic transition of the π-π conjugated system of the cation, the absorption band will expand toward hypsochromic and bathochromic shifts (i.e., blue and red shifts, respectively). The bathochromic shift originates from the J-aggregation of the chromophore cations along the *a*-axis of the crystal in a head-to-tail stacking mode, while the hypsochromic shift originates from the H-aggregation in a face-to-face stacking mode [24, 25]. The NCs

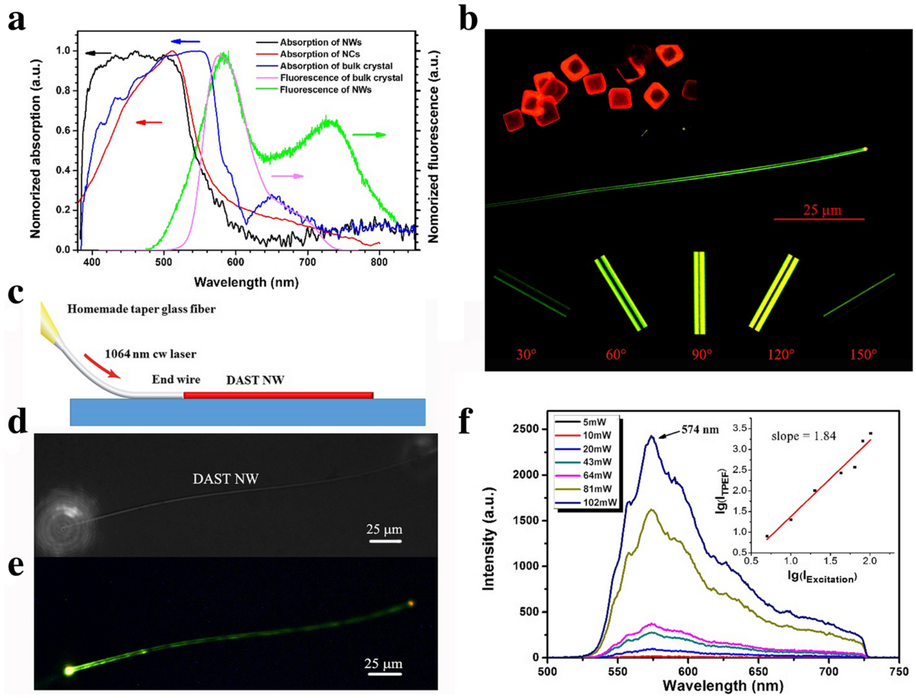

Fig. 3 **a** Absorption spectra of DAST NWs, NCs, and bulk crystals and fluorescence spectra of DAST NWs and bulk crystals excited by a 407 nm laser. **b** Fluorescence images of DAST MCs (top left), a DAST NW (center), and the DAST NW at different polarization angles (bottom). **c** Optical setup for TPEF measurements. **d** Top view of a DAST NW with 1064 nm laser input. **e** TPEF image of a DAST NW upon irradiation by the 1064 nm cw laser. **f** TPEF spectra of the DAST NW at different input laser intensities, where the inset shows the logarithm of the TPEF intensity as a function of the logarithm of the input laser intensity

exhibit only a slight expansion in the blue and red directions, as indicated by the red line in Fig. 3a with an absorption peak at ~ 512 nm, which reflects the size limitations of the two aggregation directions. In the bulk crystal case, the J- and H-aggregation lengths are significantly expanded, so the bulk crystal spectrum has the broadest absorption band, which extends from 350 nm to 750 nm, with an absorption peak at ~ 550 nm, as shown by the blue line in Fig. 3a.

In contrast, the DAST NWs, due to their well-structured 1D conformation, have an absorption band from ~ 380 nm to 600 nm, as indicated by the black line in Fig. 3a. They exhibit only a slight extension in the red direction and more significant extension in the blue direction. In other words, the NW growth does not proceed along the *a*-axis (J-aggregation direction), which is consistent with the NW morphology results. Owing to the 1D structure of the NWs, the H-aggregation is greatly enhanced, causing the NWs to exhibit similar absorption on the blue side. The fluorescence spectrum of the DAST NWs was also different from bulky DAST crystals. The spectra of DAST bulk crystals and NWs are depicted in Fig. 3a in pink and green, respectively. Since shortening the J-aggregation lengths of chromophores will cause the blue-shifted of the fluorescence spectrum [26], the DAST NWs have a spectrum more hypsochromic than that of the bulk crystals. In contrast, the cut-off wavelength on the short-wavelength side of the DAST NW spectrum is blue-shifted by ~ 30 nm. There is a new peak at ~ 730 nm, which may originate from the Fabre-Perot resonance [27] of the DAST NWs' linear structures. The fluorescence microscopy images in Fig. 3b confirm these differences.

DAST crystals with size on the order of micrometers are depicted in the upper left and appear orange upon irradiation by blue light. However, the DAST NW emits yellow-green light when irradiating under the same conditions. Besides, the end of the NW is distinctly brighter than its body, which implies that the NW confines light well; in other words, the fluorescent light was confined and enhanced by this waveguide structure [27]. The fluorescence also exhibits very strong polarity, as illustrated at the bottom of Fig. 3b, which shows polarized microscope images of a single NW rotated at various angles. Clearly, the fluorescence is altered as the rotation angle changed, which illustrates that DAST NW has strong polarized property.

We launched a 1064-nm continuous wave (cw) laser into a DAST NW through a home-made taper fiber to observe its propagation characteristics. The pump light was launched using a butt-coupling technique [26] with the setup illustrated in Fig. 3c. A top view of the propagation is shown in Fig. 3d. Since the DAST NW has ultra-fine crystal quality, there is no distinct scattering from its side walls. We could not evaluate the propagation loss because it is difficult for the NW's cut-back to change the propagation distances. The NW exhibited fluorescence even when it was irradiated by the 1064 nm cw laser. A fluorescent image of the DAST NW is presented in Fig. 3e, which emits yellow-green light which is very similar to when irradiated with blue light. We can easily confirm the 1064 nm laser propagation path since the NW absorbs the laser light and emits fluorescence. The 1064 nm laser light and the fluorescent light are well confined in the NW structure, as evidenced by the fact that the end of the NW is brighter than its side walls. The fluorescence intensity increases as the laser input increases, as shown in Fig. 3f. The dependence of the two-photon excited fluorescence (TPEF) intensity (I_{TPEF}) on the excitation intensity ($I_{\mathrm{Excitation}}$) was analyzed by taking the logarithm (lg) of each quantity. The plot of lg $I_{\mathrm{Excitation}}$ vs. lg I_{TPEF} appears in the inset of Fig. 3f, where the slope k of the fitting line is 1.84, near 2, it demonstrates the quadratic of the TPEF dependence on the excitation intensity in this measurement range. Notably, the TPEF signals were collected from the top of the NW, which was perpendicular to the light propagation direction. Along the propagation direction, the spectrum could be significantly different due to the resonance in the waveguide. The SHG signal was not observable using this setup for the following reasons: the exciting laser was launched from the end of the NW; the SHG signal collected from the top of a well-confined waveguide structure [26] is weak; the phase is mismatched in an as-grown DAST NW; the strong TPEF masked the SHG signal; and the SHG signal was in the crystal absorption band.

The crystalline features of the DAST NW were further investigated by performing SHG microscopy; the setup is shown in Fig. 4a. The SHG responses as functions of the incident laser polarization angle were collected. The inset of Fig. 4a presents a typical polar plot, where the red dots indicate the experimental data. The intensities of the parallel and vertical SHG components, I_x and I_y, respectively, can be written as

$$I_x^{2\omega} = A\ \cos 4\alpha + B\ \cos 2\alpha + C \quad (1)$$

and

$$I_y^{2\omega} = \frac{K}{2}(-\ \cos 4\alpha + 1) \quad (2)$$

Where α is the angle between the laser polarization and the long axis of the NW; A, B, and C are parameters related to the material; and K is a constant merging various parameter [28]. The solid lines in the inset of Fig. 4a represents the theoretical fits obtained using Eqs. (1) and (2). The observed SHG response has a two-lobe pattern, indicating that the anisotropy of the SHG is attributable to the intrinsic orientation of the DAST crystal. Since the SHG signal is emitted laterally from the NW [29], it is difficult to evaluate the second-order susceptibility tensors in the NW for this setup.

A DAST NW SHG image with a field size of 170x170 μm is shown in Fig. 4b where the colors represent the NW orientation angles of the crystals. The DAST NWs and MCs are distributed throughout the depicted area. Both the NWs and the crystals emit SHG signals, which indicate that both have SHG active crystal structures and similar NLO properties. The SHG signals from the

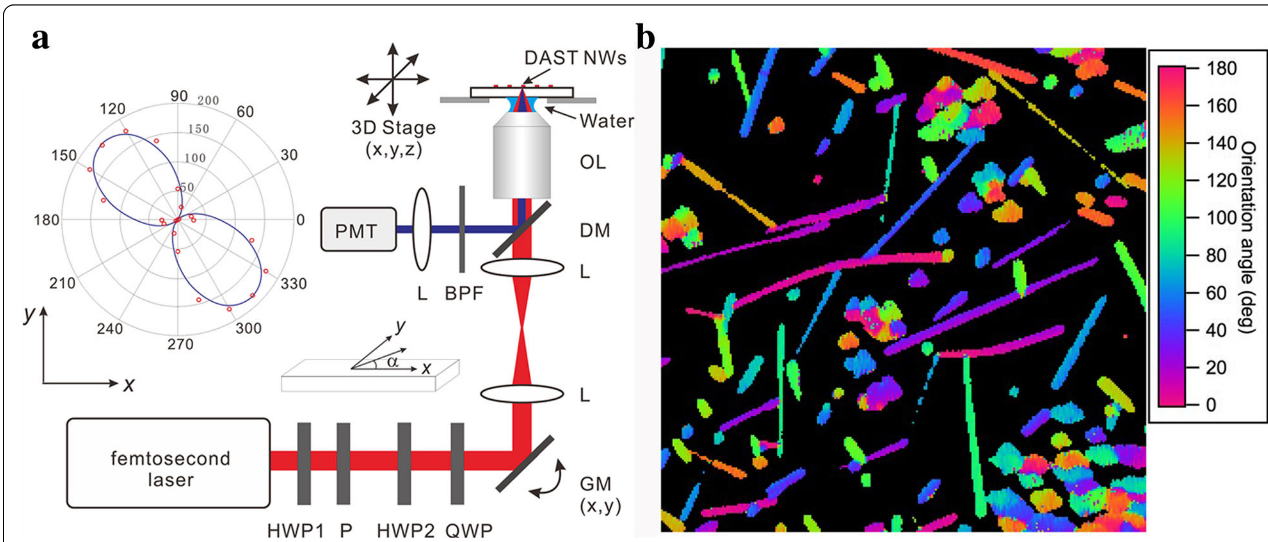

Fig. 4 a The SHG microscopy setup, where L is a lens, OL is an objective lens, DM is a dichroic mirror, GM is a galvanometer mirror, P is a polarizer, HWP is a half-wavelength polarizer, QWP is a quarter-wavelength polarizer, BPF is a band-pass filter, and PMT is a photomultiplier tube. The inset is a typical plot of the SHG intensity of a NW as a function of the incident laser polarization angle, where the red dots indicate the experimental data, and the solid blue lines represent theoretical fits. **b** SHG image of DAST NWs and their orientation angles, the field size is 170 x 170 μm

NWs are relatively uniform, which indicates the high quality of the NWs.

Conclusions

In this study, we demonstrated a one-drop self-assembling method for the DAST NWs preparation. The DAST NWs have SHG active crystal structure with very strong TPEF. The DAST NWs were observed to be single-crystalline, to have few defects, and to be well-faceted with ultra-fine surface roughness of 85 pm, which is highly beneficial for integrated device fabrication. Moreover, the method is highly efficient, the material requirement can be lower to microgram level (only 6 μg is needed in our fabrication process); thus, it is very eco-friendly.

Additional Files

Additional file 1: Figure S1. DAST NWs preparation. (DOC 2375 kb)

Abbreviations

AFM: Atomic force microscope; BTEM: Biology transmission electron microscope; CTAB: Cetyl trimethyl ammonium bromide; DAST: 4-N, N-dimethylamino-4′-N′-methyl-stilbazolium tosylate; MCs: Microcrystals; NCs: Nanocrystals; NLO: Nonlinear optical; NWs: Nanowires; SEM: Scan electron microscope; SHG: Second harmonic generation; SSREC: Substrate-supported rapid evaporation crystallization; TPEF: Two-photon excited fluorescence; XRD: X-ray diffraction

Authors' Contributions

BC conceived the experiments. TT fabricated the DAST NWs and conducted the fluorescence observations and XRD experiment. QC and TT performed the SEM measurements. YW and GX made the AFM measurements. FG, FL, and TT conducted the TPEF experiment. OS, EH, and TY performed the SHG experiment. BC wrote the manuscript in collaboration with all of the other authors.

Funding

This work was supported by the National Natural Science Foundation of China under grant no. 61377111 and NICT International Exchange Program.

Availability of Data and Materials

All the data are fully available without restrictions.

Competing Interests

The authors declare that they have no competing interests.

Author details

[1]Shanghai Key Lab of Modern Optical System, Ministry of Education, University of Shanghai for Science and Technology, Shanghai 200093, China. [2]Graduate School of Engineering, Utsunomiya University, Utsunomiya 321-8585, Japan. [3]Department of Mechanical Engineering, University of Tokushima, Tokushima, Japan.

Received: 20 March 2019 Accepted: 25 July 2019
Published online: 07 August 2019

References

1. Shi YQ, Zhang C, Zhang H, James HB, Larry RD, Bruce HR, William HS (2000) Low (sub-1-volt) halfwave voltage polymeric electro-optic modulators achieved by controlling chromophore shape. Science 288:119–122
2. Dalton LR, Sullivan PA, Bale DH (2010) Electric field poled organic electro-optic materials: state of the art and future prospects. Chem Rev 110:25–55
3. Jazbinsek M, Mutter L, Gunter P (2008) Photonic applications with the organic nonlinear optical crystal DAST. IEEE J Sel Top Quant 14:1298–1311
4. Marder SR, Perry JW, Yakymyshyn CP (1994) Organic salts with large second-order optical nonlinearities. Chem Mater 6:1137–1147
5. Katayama I, Akai R, Bito M, Shimosato H, Miyamoto K, Ito H, Ashida M (2010) Ultrabroadband Terahertz generation using 4-N, N-dimethylamino-4 ′ -N ′ 4′-N′-methyl-stilbazoliumtosylate single crystals. Appl Phys Lett 97:021105
6. Kaino T, Cai B, Takayama K (2002) Fabrication of DAST channel optical waveguide. Adv Funct Mater 12:599–603
7. Fan SZ, Qi F, Notake T, Nawata K, Matsukawa T, Takida Y, Minamide H (2014) Diffraction-limited real-time Terahertz imaging by optical frequency up-conversion in a DAST crystal. Appl Phys Lett 104:101106
8. Zheng ML, Chen WQ, Fujita K, Duan XM, Kawata S (2010) Dendrimer adjusted nanocrystals of DAST: organic crystal with enhanced nonlinear optical properties. Nanoscale 2:913–916
9. Tonouchi M (2007) Cutting-edge Terahertz technology. Nat Photonics 1:97–105
10. Meijer EW, Schenning APHJ (2002) Chemistry: material marriage in electronics. Nature 419:353–354
11. Hoeben FJM, Jonkheijm P, Meijer EW, Schenning APHJ (2005) About supramolecular assemblies of π-conjugated systems. Chem Rev 105:1491–1546
12. Yamamoto Y, Fukushima T, Suna Y, Ishii N, Saeki A, Seki S, Tagawa S, Taniguchi M, Kawai T, Aida T (2006) Photoconductive coaxial nanotubes of molecularly connected electron donor and acceptor layers. Science 314:1761–1764
13. Zhang XJ, Jie JS, Deng W, Shang QX, Wang JC, Wang H, Chen XF, Zhang XH (2016) Alignment patterning of ordered small-molecule organic semiconductor micro-/nanocrystals for device applications. Adv Mater 28:2475–2503
14. Zang L, Che Y, Moore JS (2008) One-dimensional Self-assembly of Planar π-conjugated molecules: Adaptable building blocks for organic nanodevices. Accounts Chem Res 411:1596–1608
15. Koepf M, Cherioux F, Wytko JA, Weiss J (2012) 1D and 3D surface-assisted self-organization. coordin. Chem Rev 256:2872–2892
16. Rosenne S, Grinvald E, Shirman E, Neeman L, Dutta S, Bar-Elli O, Ben-Zvi R, Oksenberg E, Milko P, Kalchenko V, Weissman H, Oron D, Rybtchinski B (2015) Self-assembled organic nanocrystals with strong nonlinear optical response. Nano Lett 15:7232–7237
17. Tian T, Cai B, Sugihara O (2016) DAST single-nanometer crystal preparation using a substrate-supported rapid evaporation crystallization method. Nanoscale 8:18882–18886
18. Tian T, Cai B, Ye TM, Cheng QQ, Zhan P, Xu GJ, Zhang L, Sugihara O (2017) One-minute self-assembly of millimetre-long DAST crystalline microbelts via substrate-supported rapid evaporation crystallization. RSC Adv 7:31691–31695
19. Oikawa H, Fujita S, Kasai H, Okada S, Tripathy SK, Nakanishi H (2000) Electric field-induced orientation of organic microcrystals with large dipole moment in dispersion liquid. Colloid Surf A-Physicochem Eng Asp 169:251–258
20. Chiang HC, Iimori T, Onodera T, Oikawa H, Ohta N (2012) Gigantic electric dipole moment of organic microcrystals evaluated in dispersion liquid with polarized electroabsorption spectra. J Phys Chem C 116:8230–8235
21. Zhang XJ, Zhang XH, Zou ZK, Lee CS, Lee ST (2007) Single-crystal nanoribbons, nanotubes, and nanowires from intramolecular charge-transfer organic molecules. J Am Chem Soc 129:3527–3532
22. Ruiz B, Jazbinsek M, Gunter P (2008) Crystal growth of DAST. Cryst Growth Des 8:4173–4184
23. Lui CH, Liu L, Mak KF, George WF (2009) Ultraflat graphene. Nature 462:339–341
24. Macchi R, Cariati E, Marinotto D, Roberto D, Tordin E, Ugo R, Bozio R, Cozzuol M, Pedron D, Mattei G (2010) Stable SHG from in situ grown oriented nanocrystals of [(E)-N, N-dimethylamino-N'-methylstilbazolium][p-toluenesulfonate] in a PMMA film. J Mater Chem 20:1885–1890
25. Miniewicz A, Palewska K, Sznitko L, Lipinski J (2011) Single-and two-photon excited fluorescence in organic nonlinear optical single crystal 3-(1,1-dicyanoethenyl)-1-phenyl-4,5-dihydro-1 h-pyrazole. J Phys Chem A 115:10689–10697
26. Gu FX, Zhang L, Wu GQ, Zhu YB, Zeng HP (2014) Sub-bandgap transverse frequency conversion in semiconductor nano-waveguides. Nanoscale 6:12371–12376
27. Zhang XL, Feng JS (2013) Spectral engineering by flexible tunings of optical Tamm states and; Fabry-Perot cavity resonance. Optics Letters 38:4382–4385

28. Gusachenko I, Latour G¨e, Claire M, Klein S (2010) Polarization-resolved second harmonic microscopy in anisotropic thick tissues. Opt Express 18: 19339–19352
29. Liu WW, Wang K, Liu Z, Shen GZ, Lu PX (2013) Laterally emitted surface second harmonic generation in a single ZnTe nanowire. Nano Lett 13:4224–4229

Publisher's Note

Springer Nature remains neutral with regard to jurisdictional claims in published maps and institutional affiliations.